High frequency, multi-axis dynamic stiffness analysis of a fractionally damped elastomeric isolator using continuous system theory

Luke Fredette, Rajendra Singh *

Acoustics and Dynamics Laboratory, Smart Vehicle Concepts Center, Department of Mechanical and Aerospace Engineering, The Ohio State University, Columbus, OH 43210, USA

ARTICLE INFO

ABSTRACT

A spectral element approach is proposed to determine the multi-axis dynamic stiffness terms of elastomeric isolators with fractional damping over a broad range of frequencies. The dynamic properties of a class of cylindrical isolators are modeled by using the continuous system theory in terms of homogeneous rods or Timoshenko beams. The transfer matrix type dynamic stiffness expressions are developed from exact harmonic solutions given translational or rotational displacement excitations. Broadband dynamic stiffness magnitudes (say up to 5 kHz) are computationally verified for axial, torsional, shear, flexural, and coupled stiffness terms using a finite element model. Some discrepancies are found between finite element and spectral element models for the axial and flexural motions, illustrating certain limitations of each method. Experimental validation is provided for an isolator with two cylindrical elements (that work primarily in the shear mode) using dynamic measurements, as reported in the prior literature, up to 600 Hz. Superiority of the fractional damping formulation over structural or viscous damping models is illustrated via experimental validation. Finally, the strengths and limitations of the spectral element approach are briefly discussed.

© 2016 Elsevier Ltd. All rights reserved.

1. Introduction

Elastomeric devices including vibration isolators are widely used in machines, equipment, and vehicles for their relatively low stiffness properties (with desired damping depending on the composition) at a relatively low cost. Prediction of their dynamic properties from basic principles is often difficult, since elastomeric materials often exhibit anisotropy, temperature- and age-dependence, as well as amplitude sensitive behavior [1–3]. As a result, dynamic stiffness at selected frequencies (and amplitudes of excitation under a given preload) are often measured using non-resonant elastomer test machines, though their operational bandwidth is often limited; even high frequency test machines are typically limited to around 500 to 1000 Hz in the uniaxial measurement mode [4,5]. However, the frequency range of interest may be much higher in many applications given vibration isolation, impedance mismatch, or acoustic comfort requirements [4–11]. Therefore, it is of vital importance to understand the isolator dynamics and its vibration transmission properties over a broad range of frequencies. Given the inherent limitations of elastomer test machines, few researchers have suggested

---

Nomenclature

A	cross-sectional area
a	left-side node (at $x = 0$)
B	translational solution coefficient
b	right-side node (at $x = L$)
C	rotational solution coefficient
c	viscous damping coefficient
D	generalized differential operator
D	diameter
E	elastic modulus
F	force
f	frequency (Hz)
G	shear modulus
H	shear equation coefficients
h	loss factor
I	second moment of area
K	dynamic stiffness
L	length
M	moment
N	number of terms
Q	generalized force
q	generalized displacement
t	time
u	translational displacement
x, y, z	coordinates or directions

α	fractional damping order
β	complex-valued wave number
γ	B to C conversion factor
ε	fractional damping coefficient
η	fractional damping coefficient
θ	rotational displacement
κ	Timoshenko shear coefficient
ν	Poisson's ratio
ρ	density
ω	circular frequency (rad/s)

Subscripts

0	static
e	excitation amplitude
m, n	matrix indices (row, column)
max	maximum bandwidth
λ	natural frequency

Abbreviations

DOF	degree(s) of freedom
FE	finite element
SEM	spectral element method

indirect methods. In particular, Noll et al. [6] estimated the stiffness properties of elastomeric isolators with three degrees of freedom (DOF) embedded in an elastic beam system from the modal properties up to around 1 kHz; however, the isolator stiffness was assumed to be spectrally invariant. Kim and Singh [7] used mobility synthesis to estimate the multi-axis dynamic properties of an isolator between two known mass elements by measuring the frequency responses of the assembled structure up to 2 kHz. Finally, Meggitt et al. [8] proposed a similar procedure to determine *in situ* isolator properties up to 2 kHz. In each case, the frequency range is restricted by experimental limitations and the underlying estimation methods.

Typically, the static and dynamic analyses in industry are conducted with commercial finite element (FE) codes. This approach has some disadvantages since many elements are required to yield accurate predictions of dynamic properties, particularly at higher frequencies. Component-level analysis of an elastomeric joint may not accurately capture its influence on a larger system, but embedding multiple high-order, FE joint type models into a larger system model can escalate the model size to an unreasonable extent. Furthermore, the usable frequency range of modal or dynamic stiffness analyses of such structures is limited by the element size, parameter uncertainty, and natural frequency spacing, suggesting the need for an analytical approach that may guide computationally intensive exercise in a more rational manner. For instance, minimal order lumped parameter models have been considered to address these difficulties with partial success over the lower frequency range [3,7,9]. However, the inertial and elastic properties are more distributed at higher frequencies or smaller wavelengths [10]. This suggests the use of continuous system methods though only certain types of solutions are tractable [11,12]. In particular, Kim and Singh [11] applied the continuous theory to flexural and longitudinal motion of an isolator, predicting the dynamic properties of elastomeric paths up to 4 kHz with the structural damping assumption. Likewise, Östberg and Kari [12] proposed a wave-guide approach for fractionally damped cylindrical isolators which achieved accurate dynamic stiffness predictions as long as the isolator length is much larger than its diameter.

This article seeks to address some of the above mentioned limitations by employing the spectral element method (SEM) to develop a coupled, 6-DOF dynamic stiffness matrix of a fractionally damped viscoelastic isolator (with a relatively short aspect ratio) up to 5 kHz, that would extend beyond the typical measurement range. The proposed method intends to offer analytical solutions that should supplement computationally expensive high-fidelity FE predictions.

2. Problem formulation

The spectral element method [13] in some ways combines features of both continuous system and minimal order models. Minimal order models have the advantage of dramatically decreased computation time, enhanced physical insight

(from more physically meaningful parameters), and simplified analytical characterization when compared to FE models. The continuous system approach typically assumes an ideal geometry (e.g. beam, plate, or shell) and obtains an exact solution to the governing equations in that structure. An exact dynamic stiffness matrix is calculated from the continuum model of a structure, but that structure may then be treated as a discrete element and even assembled within other formulations [13–19]. Such an approach requires that a structure be decomposed into basic elements suitable for continuous system analysis, but it yields accurate dynamic stiffness predictions over a very large frequency range. This approach has been used for fluid systems [14], geophysical applications [15], etc., but relatively few authors [16–19] have employed SEM to mechanical structures or elastomeric components that are common to the automotive, appliance, and aerospace industries. These often involve repetitive structures, which are particularly well suited to the SEM.

This article intends to employ linear partial differential equations to obtain a frequency-domain characterization of an isolator, thus amplitude-, preload-, and temperature-dependence are beyond the scope of this study. Such a simplification is reasonable since large amplitudes would be physically unrealistic over the medium and high frequency regimes anyway. Three damping formulations will be considered in this article since structural and viscous damping have been previously used in the SEM to compare with FE predictions. Of particular note is the fractional damping, which is regarded as a more general formulation for elastomeric materials; in fact, it has been found to be more accurate than viscous or structural damping [3,20,21]. Isolator elements will be modeled as homogeneous rods in the longitudinal and torsional direction, and as Timoshenko beams [11] for the shear and flexure directions. Specific objectives include: 1. Derive the spectral element model for fractionally damped isolator and construct multi-axis dynamic stiffness matrices, 2. Verify various dynamic stiffness terms of an elastomeric cylinder using FE models, establishing limitations in terms of aspect ratio and frequency range (up to 5 kHz), and 3. Offer experimental validation for the spectral element model of an isolator up to 600 Hz excitation [4].

The model developed in this article considers a circular rubber cylinder depicted in Fig. 1 as a basic element, from which more complicated structures may be constructed. Six degrees of freedom ($u_x, u_y, u_z, \theta_x, \theta_y, \theta_z$) are considered for each node, such as (a, b) on each side of the elastomeric material, which are assumed to be perfectly bonded to rigid surfaces. To simplify the nomenclature, generalized displacement ($\mathbf{q}$) and force ($\mathbf{Q}$) coordinates are used,

$$\mathbf{q} = \left\{ u_x, u_y, u_z, \theta_x, \theta_y, \theta_z \right\} = \left\{ q_1, q_2, q_3, q_4, q_5, q_6 \right\}, \tag{1}$$

$$\mathbf{Q} = \left\{ F_x, F_y, F_z, M_x, M_y, M_z \right\} = \left\{ Q_1, Q_2, Q_3, Q_4, Q_5, Q_6 \right\}. \tag{2}$$

Two-parameter fractional damping (Kelvin-Voigt type) is introduced, and it is embedded within the elastic modulus as,

$$E = E_0 \left(1 + \eta D_t^\alpha \right), \tag{3}$$

where E_0 is the static elastic modulus of the material, η is the fractional damping coefficient, and α is the fractional order. Here, D_t^α is a generalized fractional order differential operator,

$$D_t^\alpha = \frac{d^\alpha}{dt^\alpha}. \tag{4}$$

Additionally, the overhead tilde notation corresponds to a complex-valued quantity in the frequency domain. For instance, the elastic modulus assumes the following form,

$$\tilde{E}(\omega) = E_0 \left(1 + \eta (\mathbf{i}\omega)^\alpha \right), \tag{5}$$

applying the definition of fractional calculus in the frequency domain [20,21]. Structural damping may be viewed as a special case of the fractional damping when $\alpha = 0$, $\eta = ih$ where h is the loss factor. Viscous damping may also be considered a special case of the fractional damping when $\eta = c$ and $\alpha = 1$, where c is the viscous damping coefficient.
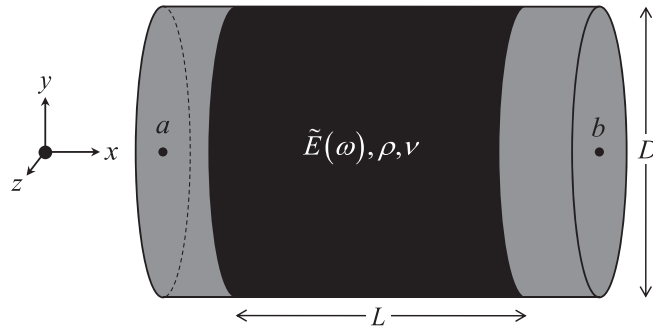

Fig. 1. Cylindrical elastomeric isolator used as the primary example. The viscoelastic material is bonded to metal end-caps, which are assumed to be rigid compared to the elastomer. Here, a and b represent the end points at $x = 0$ and $x = L$ points (nodes on each end), $\tilde{E}(\omega)$ represents the complex-valued elastic modulus, ν is the Poisson's ratio, ρ is the density of elastomeric material, D is the diameter, and L is the length.

3. Analytical formulation of the spectral element model

3.1. Combined multi-axis dynamic stiffness matrix

The full 6-DOF dynamic stiffness matrix **K**, as defined below, describes the dynamic properties of the isolator in all translational and rotational directions, including both driving-point and cross-point terms according to the transfer matrix or four pole method [22],

$$
\mathbf{K}(\omega) = \begin{bmatrix} \left[K_{ma,na} \right]_{m,n}^{6\times6} & \left[K_{ma,nb} \right]_{m,n}^{6\times6} \\ \left[K_{mb,na} \right]_{m,n}^{6\times6} & \left[K_{mb,nb} \right]_{m,n}^{6\times6} \end{bmatrix} = \begin{bmatrix} \mathbf{K}_{a,a} & \mathbf{K}_{a,b} \\ \mathbf{K}_{b,a} & \mathbf{K}_{b,b} \end{bmatrix},
\tag{6}
$$

such that

$$
\begin{Bmatrix} \mathbf{Q}_a \\ \mathbf{Q}_b \end{Bmatrix} = \mathbf{K}(\omega) \begin{Bmatrix} \mathbf{q}_a \\ \mathbf{q}_b \end{Bmatrix}.
\tag{7}
$$

Generally, each 6×6 submatrix may be fully populated where each motion or force is coupled with all others. However, if the coordinates are judiciously chosen, then each $\mathbf{K}_{m,n}$ may be rather sparse and would contain off-diagonal terms only when coupling is directly implied by the physics, such as with shear/flexure coupling in an elastic beam. Each uncoupled direction or set of coupled directions is first considered separately, and the resulting dynamic stiffness terms are then combined into the overall $\mathbf{K}(\omega)$ matrix of Eq. (6).

3.2. Axial dynamic stiffness

In the axial direction (x in Fig. 1), the longitudinal wave equation is employed in the rubber section,

$$
\frac{\partial}{\partial x}\left(EA \frac{\partial q_1}{\partial x} \right) = \rho A \frac{\partial^2 q_1}{\partial t^2},
\tag{8}
$$

where q_1 is the axial displacement, A is the cross-sectional area, and ρ is the mass density. Assuming homogeneous material properties and uniform cross-sectional geometry yields,

$$
E \frac{\partial^2 q_1}{\partial x^2} = \rho \frac{\partial^2 q_1}{\partial t^2}.
\tag{9}
$$

Assuming harmonic excitation and response (and dropping the ubiquitous $e^{i\omega t}$ term), the spatial solution and complex-valued axial wave number $\tilde{\beta}_x$ are defined in the frequency domain as follows,

$$
\tilde{q}_1(x) = \left(\tilde{B}_1 e^{\tilde{\beta}_x x} + \tilde{B}_2 e^{-\tilde{\beta}_x x} \right),
\tag{10-a}
$$

$$
\tilde{\beta}_x(\omega) = i\omega \sqrt{\frac{\rho}{\tilde{E}(\omega)}}.
\tag{10-b}
$$

The elastic axial force, assumed to be uniform throughout the cross-section, is defined,

$$
F_x = Q_1 = EA \frac{\partial q_1}{\partial x},
\tag{11}
$$

or in the frequency domain,

$$
\tilde{Q}_1(\omega) = \tilde{E} A \tilde{\beta}_x \left(\tilde{B}_1 e^{\tilde{\beta}_x x} - \tilde{B}_2 e^{-\tilde{\beta}_x x} \right).
\tag{12}
$$

Using a four-pole type formulation, the dynamic stiffness matrix at any frequency (ω) for this element can be written,

$$
\begin{Bmatrix} \tilde{Q}_{1a} \\ \tilde{Q}_{1b} \end{Bmatrix} = \begin{bmatrix} \tilde{K}_{1a,1a} & \tilde{K}_{1a,1b} \\ \tilde{K}_{1b,1a} & \tilde{K}_{1b,1b} \end{bmatrix} \begin{Bmatrix} \tilde{q}_{1a} \\ \tilde{q}_{1b} \end{Bmatrix},
\tag{13}
$$

where the "a" subscript corresponds to the location $x = 0$, "b" is at $x = L$, and the stiffness elements are determined by applying the appropriate boundary conditions as described below,

$$
\tilde{K}_{1a,1a} = \left. \frac{\tilde{Q}_{1a}}{\tilde{q}_{1a}} \right|_{\tilde{q}_{1b}=0}, \quad \tilde{K}_{1a,1b} = \left. \frac{\tilde{Q}_{1a}}{\tilde{q}_{1b}} \right|_{\tilde{q}_{1a}=0},
\tag{14-a}
$$

$$\tilde{K}_{1b,1a} = \left.\frac{\tilde{Q}_{1b}}{\tilde{q}_{1a}}\right|_{\tilde{q}_{1b}=0}, \ \tilde{K}_{1b,1b} = \left.\frac{Q_{1b}}{q_{1b}}\right|_{\tilde{q}_{1a}=0}. \tag{14-b}$$

Due to the symmetry of the structural element as shown in Fig. 1, $\tilde{K}_{1a,1b} = \tilde{K}_{1b,1a}$, and $\tilde{K}_{1a,1a} = \tilde{K}_{1b,1b}$. This symmetry would vanish if the cross-sectional area A were to vary with x. In this case, the differential Eq. (8) would no longer have constant coefficients (with respect to x), and a new type of solution would be needed. Applying boundary conditions for the cross-point dynamic stiffness in the frequency domain,

$$\tilde{q}_1(0) = 0 = \left(\tilde{B}_1 + \tilde{B}_2\right), \tag{15-a}$$

$$\tilde{q}_1(L) = q_e = \left(\tilde{B}_1 e^{i\tilde{\beta}L} + \tilde{B}_2 e^{-i\tilde{\beta}L}\right), \tag{15-b}$$

and solving for the coefficients yields,

$$\tilde{B}_1 = q_e\left(e^{i\tilde{\beta}L} - e^{-i\tilde{\beta}L}\right)^{-1}, \ \tilde{B}_2 = -\tilde{B}_1. \tag{16}$$

The cross-point and driving-point dynamic stiffness terms are then derived as,

$$\tilde{K}_{1b,1a} = \tilde{K}_{1a,1b} = \left.\frac{\tilde{Q}_{1a}}{\tilde{q}_{1b}}\right|_{q_{1a}=0} = \frac{\tilde{E}(\omega)A\tilde{\beta}_x}{\sinh\left(\tilde{\beta}_x L\right)}, \tag{17-a}$$

$$\tilde{K}_{1a,1a} = \tilde{K}_{1b,1b} = \left.\frac{\tilde{Q}_{1b}}{\tilde{q}_{1b}}\right|_{q_{1a}=0} = \frac{\tilde{E}(\omega)A\tilde{\beta}_x}{\tanh\left(\tilde{\beta}_x L\right)}. \tag{17-b}$$

3.3. Torsional dynamic stiffness

The torsional behavior of the element is similar to the axial behavior, and its coupling with other directions is assumed to be negligible. The torsional wave equation is given in terms of the torsional displacement $q_4 = \theta_x(x, t)$,

$$G\frac{\partial^2 q_4}{\partial x^2} = \rho\frac{\partial^2 q_4}{\partial t^2}, \tag{18}$$

and is recognized to be very similar to the axial wave Eq. (8), where G is the shear modulus, related to $\tilde{E}(\omega)$ and Poisson's ratio (ν) as,

$$\tilde{E}(\omega) = 2\left(1 + \nu\right)\tilde{G}(\omega). \tag{19}$$

The same harmonic solution can be used, leading to a torsional wave number,

$$\tilde{\beta}_{\theta_x}(\omega) = i\omega\sqrt{\frac{\rho}{\tilde{G}(\omega)}} = \sqrt{2\left(1 + \nu\right)}\tilde{\beta}_x. \tag{20}$$

Elastic moment is calculated,

$$M_x = Q_4 = GI_{xx}\frac{\partial q_4}{\partial x}, \tag{21}$$

where I_{xx} is the polar second moment of area. Boundary conditions for cross- and driving-point calculations are equivalent to the axial direction, symmetry is once again assumed, and the corresponding torsional dynamic stiffness terms are found to be,

$$\tilde{K}_{4b,4a} = \tilde{K}_{4a,4b} = \left.\frac{\tilde{Q}_{4a}}{\tilde{q}_{4b}}\right|_{q_{4a}=0} = \frac{\tilde{G}(\omega)I_{xx}\tilde{\beta}_{\theta_x}}{\sinh\left(\tilde{\beta}_{\theta_x} L\right)}, \tag{22-a}$$

$$\tilde{K}_{4a,4a} = \tilde{K}_{4b,4b} = \left.\frac{\tilde{Q}_{4b}}{\tilde{q}_{4b}}\right|_{q_{4a}=0} = \frac{\tilde{G}(\omega)I_{xx}\tilde{\beta}_{\theta_x}}{\tanh\left(\tilde{\beta}_{\theta_x} L\right)}. \tag{22-b}$$

3.4. Shear and flexural dynamic stiffness terms

While a no-coupling assumption is reasonable for small-amplitude, axial and torsional vibrations of the last two sub-sections, shear and bending motions must be analyzed together given strong coupling. The Timoshenko beam formulation [11] offers a robust framework for this analysis with "short" beam elements by including shear deformation and rotational

inertia. Two coupled wave equations are given for a Timoshenko beam with homogeneous material properties and a uniform cross section,

$$\kappa A G \frac{\partial}{\partial x}\left[\frac{\partial q_2}{\partial x} - q_6\right] = \rho A \frac{\partial^2 q_2}{\partial t^2},$$

(23)

$$EI_{zz}\frac{\partial^2 q_6}{\partial x^2} + \kappa A G\left[\frac{\partial q_2}{\partial x} - q_6\right] = \rho I_{zz}\frac{\partial^2 q_6}{\partial t^2},$$

(24)

for shear deformation in the y direction and bending about the z direction. Here, the geometry dependent shear coefficient κ accounts for the shear stress being not uniformly distributed on the cross section [23]. These can be combined into a single equation in terms of just one variable,

$$EI_{zz}\frac{\partial^4 q_2}{\partial x^4} + \rho A \frac{\partial^2 q_2}{\partial t^2} - \rho I_{zz}\left(1 + \frac{2(1+\nu)}{\kappa}\right)\frac{\partial^4 q_2}{\partial x^2 \partial t^2} + \frac{\rho^2 A I_{zz}}{\kappa A G}\frac{\partial^4 q_2}{\partial t^4} = 0,$$

(25)

which has the general solution,

$$\tilde{q}_2(x) = \left(\tilde{B}_{y1}e^{\tilde{\beta}_{y1}x} + \tilde{B}_{y2}e^{-\tilde{\beta}_{y1}x} + \tilde{B}_{y3}e^{\tilde{\beta}_{y2}x} + \tilde{B}_{y4}e^{-\tilde{\beta}_{y2}x}\right).$$

(26)

For the sake of compactness, Eq. (25) is rewritten as,

$$\frac{\partial^4 \tilde{q}_2}{\partial x^4} + 2\tilde{H}_2(\omega)\frac{\partial^2 \tilde{q}_2}{\partial x^2} + \tilde{H}_0(\omega)\tilde{q}_2 = 0,$$

(27)

where,

$$\tilde{H}_{y2}(\omega) = \frac{\rho\omega^2}{\tilde{E}(\omega)}\left(\frac{1}{2} + \frac{(1+\nu)}{\kappa}\right),$$

(28-a)

$$\tilde{H}_{y0}(\omega) = \frac{\rho\omega^2}{\tilde{E}(\omega)}\left(\frac{\rho\omega^2}{\kappa\tilde{G}(\omega)} - \frac{A}{I_{zz}}\right).$$

(28-b)

The following two complex-valued wave numbers emerge from the application of the quadratic formula to Eq. (27),

$$\tilde{\beta}_{y1}^2, \tilde{\beta}_{y2}^2 = -\tilde{H}_{y2} \pm \sqrt{\tilde{H}_{y2}^2 - \tilde{H}_{y0}}.$$

(29)

The rotational displacement is determined from Eq. (23),

$$\tilde{q}_6(x) = \frac{\partial \tilde{q}_2}{\partial x} + \frac{\rho\omega^2}{\kappa\tilde{G}(\omega)}\int \tilde{q}_2 \boldsymbol{dx} = \left(\tilde{C}_{y1}e^{\tilde{\beta}_{y1}x} + \tilde{C}_{y2}e^{-\tilde{\beta}_{y1}x} + \tilde{C}_{y3}e^{\tilde{\beta}_{y2}x} + \tilde{C}_{y4}e^{-\tilde{\beta}_{y2}x}\right),$$

(30-a)

$$\tilde{C}_{y1} = \left(\tilde{\beta}_{y1} + \frac{\rho\omega^2}{\kappa\tilde{G}(\omega)\tilde{\beta}_{y1}}\right)\tilde{B}_{y1} = \tilde{\gamma}_{y1}\tilde{B}_{y1},$$

(30-b)

$$\tilde{C}_{y2} = -\left(\tilde{\beta}_{y1} + \frac{\rho\omega^2}{\kappa\tilde{G}(\omega)\tilde{\beta}_{y1}}\right)\tilde{B}_{y2} = -\tilde{\gamma}_{y1}\tilde{B}_{y2},$$

(30-c)

$$\tilde{C}_{y3} = \left(\tilde{\beta}_{y2} + \frac{\rho\omega^2}{\kappa\tilde{G}(\omega)\tilde{\beta}_{y2}}\right)\tilde{B}_{y3} = \tilde{\gamma}_{y2}\tilde{B}_{y3},$$

(30-d)

$$\tilde{C}_{y4} = -\left(\tilde{\beta}_{y2} + \frac{\rho\omega^2}{\kappa\tilde{G}(\omega)\tilde{\beta}_{y2}}\right)\tilde{B}_{y4} = -\tilde{\gamma}_{y2}\tilde{B}_{y4}.$$

(30-e)

Shear force and bending moment are defined,

$$F_y = Q_2 = \kappa A G\left(\frac{\partial q_2}{\partial x} - q_6\right),$$

(31)

$$M_z = Q_6 = -EI_{zz}\frac{\partial q_6}{\partial x}.$$
(32)

Since there are two degrees of freedom at each node, the dynamic stiffness matrix must be of dimension 4. Three fixed displacements and one applied force boundary condition are applied for each dynamic stiffness term. For a translational harmonic displacement input,

$$\tilde{q}_2(0) = 0 = \tilde{B}_{y1} + \tilde{B}_{y2} + \tilde{B}_{y3} + \tilde{B}_{y4},$$
(33-a)

$$\tilde{q}_2(L) = q_e = \left(\tilde{B}_{y1}e^{\tilde{\beta}_{y1}L} + \tilde{B}_{y2}e^{-\tilde{\beta}_{y1}L} + \tilde{B}_{y3}e^{\tilde{\beta}_{y2}L} + \tilde{B}_{y4}e^{-\tilde{\beta}_{y2}L}\right),$$
(33-b)

$$\tilde{q}_6(0) = 0 = \tilde{C}_{y1} + \tilde{C}_{y2} + \tilde{C}_{y3} + \tilde{C}_{y4},$$
(33-c)

$$\tilde{q}_6(L) = 0 = \tilde{C}_{y1}e^{\tilde{\beta}_{y1}L} + \tilde{C}_{y2}e^{-\tilde{\beta}_{y1}L} + \tilde{C}_{y3}e^{\tilde{\beta}_{y2}L} + \tilde{C}_{y4}e^{-\tilde{\beta}_{y2}L},$$
(33-d)

or in matrix form,

$$\begin{bmatrix} 1 & 1 & 1 & 1 \\ e^{\tilde{\beta}_{y1}L} & e^{-\tilde{\beta}_{y1}L} & e^{\tilde{\beta}_{y2}L} & e^{-\tilde{\beta}_{y2}L} \\ \tilde{\gamma}_{y1} & -\tilde{\gamma}_{y1} & \tilde{\gamma}_{y2} & -\tilde{\gamma}_{y2} \\ \tilde{\gamma}_{y1}e^{\tilde{\beta}_{y1}L} & -\tilde{\gamma}_{y1}e^{-\tilde{\beta}_{y1}L} & \tilde{\gamma}_{y2}e^{\tilde{\beta}_{y2}L} & -\tilde{\gamma}_{y2}e^{-\tilde{\beta}_{y2}L} \end{bmatrix} \begin{Bmatrix} \tilde{B}_{y1} \\ \tilde{B}_{y2} \\ \tilde{B}_{y3} \\ \tilde{B}_{y4} \end{Bmatrix} = \begin{Bmatrix} 0 \\ q_e \\ 0 \\ 0 \end{Bmatrix}.$$
(34)

The $\tilde{B}$ coefficients may be explicitly calculated from this equation using Cramer's rule, direct matrix inversion, or a symbolic solver. For the sake of brevity, the resulting expressions are not explicitly given. The dynamic stiffness terms are found as,

$$\tilde{K}_{2a,2a} = \tilde{K}_{2b,2b} = \frac{\tilde{Q}_{2b}}{\tilde{q}_{2b}}\bigg|_{\tilde{q}_{2a},\tilde{q}_{6a},\tilde{q}_{6b}=0} = \frac{\kappa A \tilde{G}\left(\begin{array}{c}\tilde{B}_{y1}(\tilde{\beta}_{y1}-\tilde{\gamma}_{y1})e^{\tilde{\beta}_{y1}L} - \tilde{B}_{y2}(\tilde{\beta}_{y1}-\tilde{\gamma}_{y1})e^{-\tilde{\beta}_{y1}L} \\ +\tilde{B}_{y3}(\tilde{\beta}_{y2}-\tilde{\gamma}_{y2})e^{\tilde{\beta}_{y2}L} - \tilde{B}_{y4}(\tilde{\beta}_{y2}-\tilde{\gamma}_{y2})e^{-\tilde{\beta}_{y2}L}\end{array}\right)}{\left(\tilde{B}_{y1}e^{\tilde{\beta}_{y1}L} + \tilde{B}_{y2}e^{-\tilde{\beta}_{y1}L} + \tilde{B}_{y3}e^{\tilde{\beta}_{y2}L} + \tilde{B}_{y4}e^{-\tilde{\beta}_{y2}L}\right)},$$
(35-a)

$$\tilde{K}_{2b,2a} = \tilde{K}_{2a,2b} = \frac{\tilde{Q}_{2a}}{\tilde{q}_{2b}}\bigg|_{\tilde{q}_{2a},\tilde{q}_{6a},\tilde{q}_{6b}=0} = \frac{\kappa A \tilde{G}\left(\begin{array}{c}\tilde{B}_{y1}(\tilde{\beta}_{y1}-\tilde{\gamma}_{y1}) - \tilde{B}_{y2}(\tilde{\beta}_{y1}-\tilde{\gamma}_{y1}) \\ +\tilde{B}_{y3}(\tilde{\beta}_{y2}-\tilde{\gamma}_{y2}) - \tilde{B}_{y4}(\tilde{\beta}_{y2}-\tilde{\gamma}_{y2})\end{array}\right)}{\left(\tilde{B}_{y1}e^{\tilde{\beta}_{y1}L} + \tilde{B}_{y2}e^{-\tilde{\beta}_{y1}L} + \tilde{B}_{y3}e^{\tilde{\beta}_{y2}L} + \tilde{B}_{y4}e^{-\tilde{\beta}_{y2}L}\right)},$$
(35-b)

$$\tilde{K}_{6a,2a} = \tilde{K}_{6b,2b} = \frac{\tilde{Q}_{6b}}{\tilde{q}_{2b}}\bigg|_{\tilde{q}_{2a},\tilde{q}_{6a},\tilde{q}_{6b}=0} = \frac{-\tilde{E}I_{zz}\left(\begin{array}{c}\tilde{\beta}_{y1}\tilde{\gamma}_{y1}\tilde{B}_{y1}e^{\tilde{\beta}_{y1}L} + \tilde{\beta}_{y1}\tilde{\gamma}_{y1}\tilde{B}_{y2}e^{-\tilde{\beta}_{y1}L} \\ +\tilde{\beta}_{y2}\tilde{\gamma}_{y2}\tilde{B}_{y3}e^{\tilde{\beta}_{y2}L} + \tilde{\beta}_{y2}\tilde{\gamma}_{y2}\tilde{B}_{y4}e^{-\tilde{\beta}_{y2}L}\end{array}\right)}{\left(\tilde{B}_{y1}e^{\tilde{\beta}_{y1}L} + \tilde{B}_{y2}e^{-\tilde{\beta}_{y1}L} + \tilde{B}_{y3}e^{\tilde{\beta}_{y2}L} + \tilde{B}_{y4}e^{-\tilde{\beta}_{y2}L}\right)},$$
(35-c)

$$\tilde{K}_{6b,2a} = \tilde{K}_{6a,2b} = \frac{\tilde{Q}_{6a}}{\tilde{q}_{2b}}\bigg|_{\tilde{q}_{2a},\tilde{q}_{6a},\tilde{q}_{6b}=0} = \frac{-\tilde{E}I_{zz}\left(\tilde{\beta}_{y1}\tilde{\gamma}_{y1}\tilde{B}_{y1} + \tilde{\beta}_{y1}\tilde{\gamma}_{y1}\tilde{B}_{y2} + \tilde{\beta}_{y2}\tilde{\gamma}_{y2}\tilde{B}_{y3} + \tilde{\beta}_{y2}\tilde{\gamma}_{y2}\tilde{B}_{y4}\right)}{\left(\tilde{B}_{y1}e^{\tilde{\beta}_{y1}L} + \tilde{B}_{y2}e^{-\tilde{\beta}_{y1}L} + \tilde{B}_{y3}e^{\tilde{\beta}_{y2}L} + \tilde{B}_{y4}e^{-\tilde{\beta}_{y2}L}\right)}.$$
(35-d)

For a harmonic rotational displacement input,

$$\tilde{q}_2(0) = 0 = \tilde{B}_{y1} + \tilde{B}_{y2} + \tilde{B}_{y3} + \tilde{B}_{y4},$$
(36-a)

$$\tilde{q}_2(L) = 0 = \tilde{B}_{y1}e^{\tilde{\beta}_{y1}L} + \tilde{B}_{y2}e^{-\tilde{\beta}_{y1}L} + \tilde{B}_{y3}e^{\tilde{\beta}_{y2}L} + \tilde{B}_{y4}e^{-\tilde{\beta}_{y2}L},$$
(36-b)

$$\tilde{q}_6(0) = 0 = \tilde{C}_{y1} + \tilde{C}_{y2} + \tilde{C}_{y3} + \tilde{C}_{y4},$$
(36-c)

$$\tilde{q}_6(L) = q_e = \left(\tilde{C}_{y1}e^{\tilde{\beta}_{y1}L} + \tilde{C}_{y2}e^{-\tilde{\beta}_{y1}L} + \tilde{C}_{y3}e^{\tilde{\beta}_{y2}L} + \tilde{C}_{y4}e^{-\tilde{\beta}_{y2}L}\right),$$
(36-d)

or again in matrix form,

$$\begin{bmatrix} 1 & 1 & 1 & 1 \\ e^{\tilde{\beta}_{y1}L} & e^{-\tilde{\beta}_{y1}L} & e^{\tilde{\beta}_{y2}L} & e^{-\tilde{\beta}_{y2}L} \\ \tilde{\gamma}_{y1} & -\tilde{\gamma}_{y1} & \tilde{\gamma}_{y2} & -\tilde{\gamma}_{y2} \\ \tilde{\gamma}_{y1}e^{\tilde{\beta}_{y1}L} & -\tilde{\gamma}_{y1}e^{-\tilde{\beta}_{y1}L} & \tilde{\gamma}_{y2}e^{\tilde{\beta}_{y2}L} & -\tilde{\gamma}_{y2}e^{-\tilde{\beta}_{y2}L} \end{bmatrix} \begin{Bmatrix} \tilde{B}_{y1} \\ \tilde{B}_{y2} \\ \tilde{B}_{y3} \\ \tilde{B}_{y4} \end{Bmatrix} = \begin{Bmatrix} 0 \\ 0 \\ 0 \\ q_e \end{Bmatrix}. \tag{37}$$

The dynamic stiffness terms are then determined as,

$$\tilde{K}_{6a,6a} = \tilde{K}_{6b,6b} = \frac{\tilde{Q}_{6b}}{\tilde{q}_{6b}}\Bigg|_{\tilde{q}_{2a},\tilde{q}_{2b},\tilde{q}_{6a}=0} = \frac{-\tilde{E}I_{zz}\left(\tilde{\beta}_{y1}\tilde{C}_{y1}e^{\tilde{\beta}_{y1}L} - \tilde{\beta}_{y1}\tilde{C}_{y2}e^{-\tilde{\beta}_{y1}L} + \tilde{\beta}_{y2}\tilde{C}_{y3}e^{\tilde{\beta}_{y2}L} - \tilde{\beta}_{y2}\tilde{C}_{y4}e^{-\tilde{\beta}_{y2}L}\right)}{\left(\tilde{C}_{y1}e^{\tilde{\beta}_{y1}L} + \tilde{C}_{y2}e^{-\tilde{\beta}_{y1}L} + \tilde{C}_{y3}e^{\tilde{\beta}_{y2}L} + \tilde{C}_{y4}e^{-\tilde{\beta}_{y2}L}\right)}, \tag{38-a}$$

$$\tilde{K}_{6b,6a} = \tilde{K}_{6a,6b} = \frac{\tilde{Q}_{6a}}{\tilde{q}_{6b}}\Bigg|_{\tilde{q}_{2a},\tilde{q}_{2b},\tilde{q}_{6a}=0} = \frac{-\tilde{E}I_{zz}\left(\tilde{\beta}_{y1}\tilde{C}_{y1} - \tilde{\beta}_{y1}\tilde{C}_{y2} + \tilde{\beta}_{y2}\tilde{C}_{y3} - \tilde{\beta}_{y2}\tilde{C}_{y4}\right)}{\left(\tilde{C}_{y1}e^{\tilde{\beta}_{y1}L} + \tilde{C}_{y2}e^{-\tilde{\beta}_{y1}L} + \tilde{C}_{y3}e^{\tilde{\beta}_{y2}L} + \tilde{C}_{y4}e^{-\tilde{\beta}_{y2}L}\right)}, \tag{38-b}$$

$$\tilde{K}_{2a,6a} = \tilde{K}_{2b,6b} = \frac{\tilde{Q}_{2b}}{\tilde{q}_{6b}}\Bigg|_{\tilde{q}_{2a},\tilde{q}_{2b},\tilde{q}_{6a}=0} = \kappa A\tilde{G}\left(\frac{\tilde{\beta}_{y1}\tilde{B}_{y1}e^{\tilde{\beta}_{y1}L} - \tilde{\beta}_{y1}\tilde{B}_{y2}e^{-\tilde{\beta}_{y1}L} + \tilde{\beta}_{y2}\tilde{B}_{y3}e^{\tilde{\beta}_{y2}L} - \tilde{\beta}_{y2}\tilde{B}_{y4}e^{-\tilde{\beta}_{y2}L}}{\tilde{C}_{y1}e^{\tilde{\beta}_{y1}L} + \tilde{C}_{y2}e^{-\tilde{\beta}_{y1}L} + \tilde{C}_{y3}e^{\tilde{\beta}_{y2}L} + \tilde{C}_{y4}e^{-\tilde{\beta}_{y2}L}} - 1\right), \tag{38-c}$$

$$\tilde{K}_{2b,6a} = \tilde{K}_{2a,6b} = \frac{\tilde{Q}_{2a}}{\tilde{q}_{6b}}\Bigg|_{\tilde{q}_{2a},\tilde{q}_{2b},\tilde{q}_{6a}=0} = \frac{\kappa A\tilde{G}\left(\left(\tilde{\beta}_{y1} - \tilde{\gamma}_{y1}\right)\tilde{B}_{y1} - \left(\tilde{\beta}_{y1} - \tilde{\gamma}_{y1}\right)\tilde{B}_{y2} + \left(\tilde{\beta}_{y2} - \tilde{\gamma}_{y2}\right)\tilde{B}_{y3} - \left(\tilde{\beta}_{y2} - \tilde{\gamma}_{y2}\right)\tilde{B}_{y4}\right)}{\left(\tilde{C}_{y1}e^{\tilde{\beta}_{y1}L} + \tilde{C}_{y2}e^{-\tilde{\beta}_{y1}L} + \tilde{C}_{y3}e^{\tilde{\beta}_{y2}L} + \tilde{C}_{y4}e^{-\tilde{\beta}_{y2}L}\right)}. \tag{38-d}$$

For shear in the z direction and coupled bending about the y axis, an analogous procedure is used, but the sense of the flexural direction is reversed. The Timoshenko beam equations assume that the cross product of unit vectors in the axial and shear directions will result in the bending direction [13]. However, it is clear that $\vec{x} \times \vec{z} = -\vec{y}$, so $-\theta_y$ (rather than θ_y) must be used as the flexural coordinate. The solutions follow the same exponential form,

$$\tilde{q}_3(x) = \left(\tilde{B}_{z1}e^{\tilde{\beta}_{z1}x} + \tilde{B}_{z2}e^{-\tilde{\beta}_{z1}x} + \tilde{B}_{z3}e^{\tilde{\beta}_{z2}x} + \tilde{B}_{z4}e^{-\tilde{\beta}_{z2}x}\right), \tag{39-a}$$

$$\tilde{q}_5(x) = \left(\tilde{C}_{z1}e^{\tilde{\beta}_{z1}x} + \tilde{C}_{z2}e^{-\tilde{\beta}_{z1}x} + \tilde{C}_{z3}e^{\tilde{\beta}_{z2}x} + \tilde{C}_{z4}e^{-\tilde{\beta}_{z2}x}\right). \tag{39-b}$$

The wave numbers are defined, also as before,

$$\tilde{H}_{z2}(\omega) = \frac{\omega^2\rho}{\tilde{E}(\omega)}\left(\frac{1}{2} + \frac{(1+\nu)}{\kappa}\right), \tag{40-a}$$

$$\tilde{H}_{z0}(\omega) = \frac{\rho}{\tilde{E}(\omega)}\left(\frac{\omega^4\rho}{\kappa\tilde{G}(\omega)} - \frac{\omega^2A}{I_{yy}}\right), \tag{40-b}$$

$$\tilde{\beta}_{z1}^2, \tilde{\beta}_{z2}^2 = -\tilde{H}_{z2} \pm \sqrt{\tilde{H}_{z2}^2 - \tilde{H}_{z0}}, \tag{41}$$

and since the angle has the opposite sense, the $\tilde{C}$ coefficients are defined,

$$\tilde{C}_{z1} = -\left(\tilde{\beta}_{z1} + \frac{\rho\omega^2}{\tilde{G}(\omega)\tilde{\beta}_{z1}}\right)\tilde{B}_{z1} = \tilde{\gamma}_{z1}\tilde{B}_{z1}, \tag{42-a}$$

$$\tilde{C}_{z2} = \left(\tilde{\beta}_{z1} + \frac{\rho\omega^2}{\tilde{G}(\omega)\tilde{\beta}_{z1}}\right)\tilde{B}_{z2} = -\tilde{\gamma}_{z1}\tilde{B}_{z2}, \tag{42-b}$$

$$\tilde{C}_{z3} = -\left(\tilde{\beta}_{z2} + \frac{\rho\omega^2}{\tilde{G}(\omega)\tilde{\beta}_{z2}}\right)\tilde{B}_{z3} = \tilde{\gamma}_{z2}\tilde{B}_{z3}, \tag{42-c}$$

$$\tilde{C}_{z4} = -\left(\tilde{\beta}_{z2} + \frac{\rho\omega^2}{\tilde{G}(\omega)\tilde{\beta}_{z2}}\right)\tilde{B}_{z4} = -\tilde{\gamma}_{z2}\tilde{B}_{z4}. \tag{42-d}$$

Analogous boundary conditions are applied, beginning with a translational displacement,

Table 1
Physical properties for finite element and spectral element studies of the isolator of Fig. 1.

Property	Value
E_0	8 MPa
ν	0.48
ρ	1.1 kg/m³
h	0.1

$$\begin{bmatrix} 1 & 1 & 1 & 1 \\ e^{\tilde{\beta}_{z1}L} & e^{-\tilde{\beta}_{z1}L} & e^{\tilde{\beta}_{z2}L} & e^{-\tilde{\beta}_{z2}L} \\ \tilde{\gamma}_{z1} & -\tilde{\gamma}_{z1} & \tilde{\gamma}_{z2} & -\tilde{\gamma}_{z2} \\ \tilde{\gamma}_{z1}e^{\tilde{\beta}_{z1}L} & -\tilde{\gamma}_{z1}e^{-\tilde{\beta}_{z1}L} & \tilde{\gamma}_{z2}e^{\tilde{\beta}_{z2}L} & -\tilde{\gamma}_{z2}e^{-\tilde{\beta}_{z2}L} \end{bmatrix} \begin{Bmatrix} \tilde{B}_{z1} \\ \tilde{B}_{z2} \\ \tilde{B}_{z3} \\ \tilde{B}_{z4} \end{Bmatrix} = \begin{Bmatrix} 0 \\ q_e \\ 0 \\ 0 \end{Bmatrix}, \tag{43}$$

leading to the following dynamic stiffness terms,

$$\tilde{K}_{3a,3a} = \tilde{K}_{3b,3b} = \frac{\tilde{Q}_{3b}}{\tilde{q}_{3b}}\bigg|_{\tilde{q}_{3a},\tilde{q}_{5a},\tilde{q}_{5b}=0} = \frac{\kappa A\tilde{G}\begin{pmatrix} \tilde{B}_{z1}(\tilde{\beta}_{z1}-\tilde{\gamma}_{z1})e^{\tilde{\beta}_{z1}L} - \tilde{B}_{z2}(\tilde{\beta}_{z1}-\tilde{\gamma}_{z1})e^{-\tilde{\beta}_{z1}L} \\ +\tilde{B}_{z3}(\tilde{\beta}_{z2}-\tilde{\gamma}_{z2})e^{\tilde{\beta}_{z2}L} - \tilde{B}_{z4}(\tilde{\beta}_{z2}-\tilde{\gamma}_{z2})e^{-\tilde{\beta}_{z2}L} \end{pmatrix}}{\left(\tilde{B}_{z1}e^{\tilde{\beta}_{z1}L} + \tilde{B}_{z2}e^{-\tilde{\beta}_{z1}L} + \tilde{B}_{z3}e^{\tilde{\beta}_{z2}L} + \tilde{B}_{z4}e^{-\tilde{\beta}_{z2}L}\right)}, \tag{44-a}$$

$$\tilde{K}_{3b,3a} = \tilde{K}_{3a,3b} = \frac{\tilde{Q}_{3a}}{\tilde{q}_{3b}}\bigg|_{\tilde{q}_{3a},\tilde{q}_{5a},\tilde{q}_{5b}=0} = \frac{\kappa A\tilde{G}\begin{pmatrix} \tilde{B}_{z1}(\tilde{\beta}_{z1}-\tilde{\gamma}_{z1}) - \tilde{B}_{z2}(\tilde{\beta}_{z1}-\tilde{\gamma}_{z1}) \\ +\tilde{B}_{z3}(\tilde{\beta}_{z2}-\tilde{\gamma}_{z2}) - \tilde{B}_{z4}(\tilde{\beta}_{z2}-\tilde{\gamma}_{z2}) \end{pmatrix}}{\left(\tilde{B}_{z1}e^{\tilde{\beta}_{z1}L} + \tilde{B}_{z2}e^{-\tilde{\beta}_{z1}L} + \tilde{B}_{z3}e^{\tilde{\beta}_{z2}L} + \tilde{B}_{z4}e^{-\tilde{\beta}_{z2}L}\right)}, \tag{44-b}$$

$$\tilde{K}_{5a,3a} = \tilde{K}_{5b,3b} = \frac{\tilde{Q}_{5b}}{\tilde{q}_{3b}}\bigg|_{\tilde{q}_{3a},\tilde{q}_{5a},\tilde{q}_{5b}=0} = \frac{-\tilde{E}I_{yy}\begin{pmatrix} \tilde{\beta}_{z1}\tilde{\gamma}_{z1}\tilde{B}_{z1}e^{\tilde{\beta}_{z1}L} + \tilde{\beta}_{z1}\tilde{\gamma}_{z1}\tilde{B}_{z2}e^{-\tilde{\beta}_{z1}L} \\ +\tilde{\beta}_{z2}\tilde{\gamma}_{z2}\tilde{B}_{z3}e^{\tilde{\beta}_{z2}L} + \tilde{\beta}_{z2}\tilde{\gamma}_{z2}\tilde{B}_{z4}e^{-\tilde{\beta}_{z2}L} \end{pmatrix}}{\left(\tilde{B}_{z1}e^{\tilde{\beta}_{z1}L} + \tilde{B}_{z2}e^{-\tilde{\beta}_{z1}L} + \tilde{B}_{z3}e^{\tilde{\beta}_{z2}L} + \tilde{B}_{z4}e^{-\tilde{\beta}_{z2}L}\right)}, \tag{44-c}$$

$$\tilde{K}_{5b,3a} = \tilde{K}_{5a,3b} = \frac{\tilde{Q}_{5a}}{\tilde{q}_{3b}}\bigg|_{\tilde{q}_{3a},\tilde{q}_{5a},\tilde{q}_{5b}=0} = \frac{-\tilde{E}I_{yy}\left(\tilde{\beta}_{z1}\tilde{\gamma}_{z1}\tilde{B}_{z1} + \tilde{\beta}_{z1}\tilde{\gamma}_{z1}\tilde{B}_{z2} + \tilde{\beta}_{z2}\tilde{\gamma}_{z2}\tilde{B}_{z3} + \tilde{\beta}_{z2}\tilde{\gamma}_{z2}\tilde{B}_{z4}\right)}{\left(\tilde{B}_{z1}e^{\tilde{\beta}_{z1}L} + \tilde{B}_{z2}e^{-\tilde{\beta}_{z1}L} + \tilde{B}_{z3}e^{\tilde{\beta}_{z2}L} + \tilde{B}_{z4}e^{-\tilde{\beta}_{z2}L}\right)}. \tag{44-d}$$

Under a rotational displacement excitation, the following boundary conditions are applied,

$$\begin{bmatrix} 1 & 1 & 1 & 1 \\ e^{\tilde{\beta}_{z1}L} & e^{-\tilde{\beta}_{z1}L} & e^{\tilde{\beta}_{z2}L} & e^{-\tilde{\beta}_{z2}L} \\ \tilde{\gamma}_{z1} & -\tilde{\gamma}_{z1} & \tilde{\gamma}_{z2} & -\tilde{\gamma}_{z2} \\ \tilde{\gamma}_{z1}e^{\tilde{\beta}_{z1}L} & \tilde{\gamma}_{z1}e^{-\tilde{\beta}_{z1}L} & \tilde{\gamma}_{z2}e^{\tilde{\beta}_{z2}L} & \tilde{\gamma}_{z2}e^{-\tilde{\beta}_{z2}L} \end{bmatrix} \begin{Bmatrix} \tilde{B}_{z1} \\ \tilde{B}_{z2} \\ \tilde{B}_{z3} \\ \tilde{B}_{z4} \end{Bmatrix} = \begin{Bmatrix} 0 \\ 0 \\ 0 \\ q_e \end{Bmatrix}, \tag{45}$$

leading to the last set of dynamic stiffness terms,

$$\tilde{K}_{5a,5a} = \tilde{K}_{5b,5b} = \frac{\tilde{Q}_{5b}}{\tilde{q}_{5b}}\bigg|_{\tilde{q}_{3a},\tilde{q}_{3b},\tilde{q}_{5a}=0} = \frac{-\tilde{E}I_{yy}\left(\tilde{\beta}_{z1}\tilde{C}_{z1}e^{\tilde{\beta}_{z1}L} - \tilde{\beta}_{z1}\tilde{C}_{z2}e^{-\tilde{\beta}_{z1}L} + \tilde{\beta}_{z2}\tilde{C}_{z3}e^{\tilde{\beta}_{z2}L} - \tilde{\beta}_{z2}\tilde{C}_{z4}e^{-\tilde{\beta}_{z2}L}\right)}{\left(\tilde{C}_{z1}e^{\tilde{\beta}_{z1}L} + \tilde{C}_{z2}e^{-\tilde{\beta}_{z1}L} + \tilde{C}_{z3}e^{\tilde{\beta}_{z2}L} + \tilde{C}_{z4}e^{-\tilde{\beta}_{z2}L}\right)}, \tag{46-a}$$

$$\tilde{K}_{5b,5a} = \tilde{K}_{5a,5b} = \frac{\tilde{Q}_{5a}}{\tilde{q}_{5b}}\bigg|_{\tilde{q}_{3a},\tilde{q}_{3b},\tilde{q}_{5a}=0} = \frac{-\tilde{E}I_{yy}\left(\tilde{\beta}_{z1}\tilde{C}_{z1} - \tilde{\beta}_{z1}\tilde{C}_{z2} + \tilde{\beta}_{z2}\tilde{C}_{z3} - \tilde{\beta}_{z2}\tilde{C}_{z4}\right)}{\left(\tilde{C}_{z1}e^{\tilde{\beta}_{z1}L} + \tilde{C}_{z2}e^{-\tilde{\beta}_{z1}L} + \tilde{C}_{z3}e^{\tilde{\beta}_{z2}L} + \tilde{C}_{z4}e^{-\tilde{\beta}_{z2}L}\right)}, \tag{46-b}$$
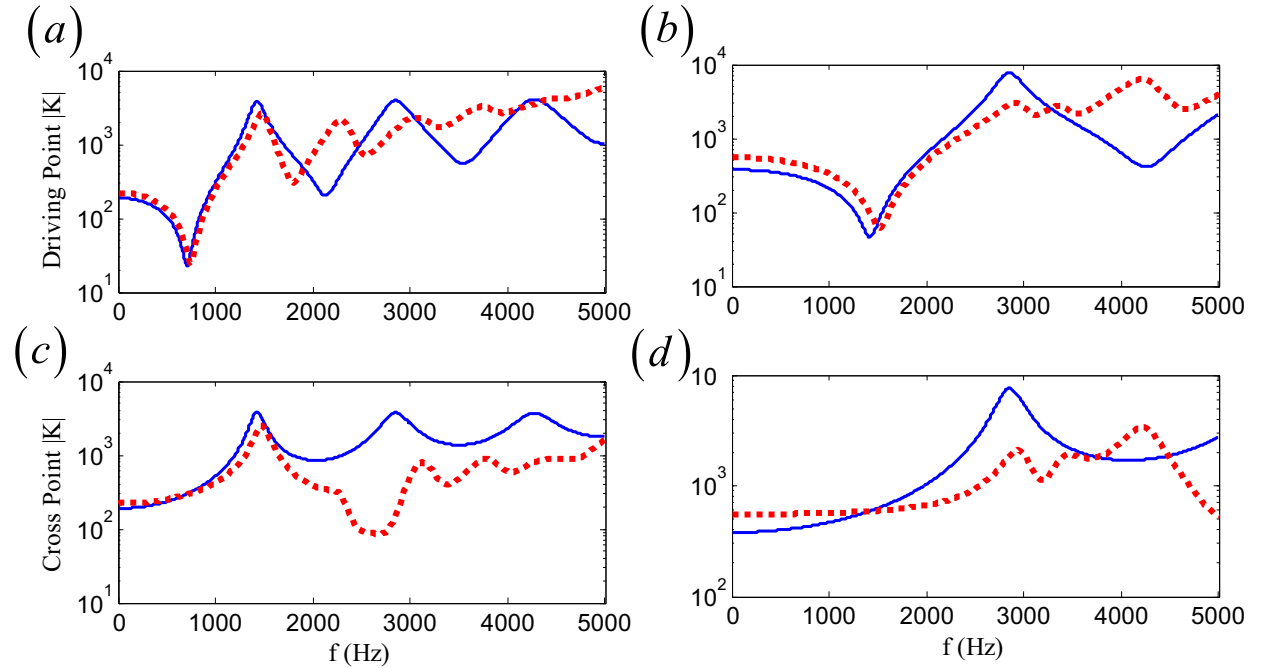
$$\tilde{K}_{3a,5a} = \tilde{K}_{3b,5b} = \frac{\tilde{Q}_{3b}}{\tilde{q}_{5b}}\bigg|_{\tilde{q}_{3a},\tilde{q}_{3b},\tilde{q}_{5a}=0} = \kappa A\tilde{G}\left(\frac{\tilde{\beta}_{z1}\tilde{B}_{z1}e^{\tilde{\beta}_{z1}L} - \tilde{\beta}_{z1}\tilde{B}_{z2}e^{-\tilde{\beta}_{z1}L} + \tilde{\beta}_{z2}\tilde{B}_{z3}e^{\tilde{\beta}_{z2}L} - \tilde{\beta}_{z2}\tilde{B}_{z4}e^{-\tilde{\beta}_{z2}L}}{\tilde{C}_{z1}e^{\tilde{\beta}_{z1}L} + \tilde{C}_{z2}e^{-\tilde{\beta}_{z1}L} + \tilde{C}_{z3}e^{\tilde{\beta}_{z2}L} + \tilde{C}_{z4}e^{-\tilde{\beta}_{z2}L}} - 1\right), \tag{46-c}$$

$$\tilde{K}_{3b,5a} = \tilde{K}_{3a,5b} = \frac{\tilde{Q}_{3a}}{\tilde{q}_{5b}}\bigg|_{\tilde{q}_{3a},\tilde{q}_{3b},\tilde{q}_{5a}=0} = \frac{\kappa A\tilde{G}\left((\tilde{\beta}_{z1}-\tilde{\gamma}_{z1})\tilde{B}_{z1} - (\tilde{\beta}_{z1}-\tilde{\gamma}_{z1})\tilde{B}_{z2} + (\tilde{\beta}_{z2}-\tilde{\gamma}_{z2})\tilde{B}_{z3} - (\tilde{\beta}_{z2}-\tilde{\gamma}_{z2})\tilde{B}_{z4}\right)}{\left(\tilde{C}_{z1}e^{\tilde{\beta}_{z1}L} + \tilde{C}_{z2}e^{-\tilde{\beta}_{z1}L} + \tilde{C}_{z3}e^{\tilde{\beta}_{z2}L} + \tilde{C}_{z4}e^{-\tilde{\beta}_{z2}L}\right)}. \tag{46-d}$$

Table 2
Parameters used for the finite element study of the isolator of Fig. 1.

Aspect Ratio (L/D)	D (mm)	L (mm)	Number of elements employed
4	30	120	4480
2	30	60	2320
1	30	30	4080
3/4	30	22.5	1970
1/2	30	15	4820
1/4	30	7.5	16180

Fig. 2. Axial dynamic stiffness spectra for the isolator of Fig. 1. With values listed in Table 1. (a)K_{1a1a} with unity aspect ratio ($L/D = 1$), (b)K_{1a1a} with short aspect ratio ($L/D = 1/2$), (c)K_{1a1b} with $L/D = 1$, (a)K_{1a1b} with $L/D = 1/2$. Key: —— – spectral element model; ■ ■ ■ – finite element model.

4. Verification of dynamic stiffness expressions using finite element models

A finite element study is carried out as verification for the spectral element model. A cylindrical rubber isolator similar to the one depicted in Fig. 1 is taken with two aspect ratios (L/D) as example cases and their properties are given in Table 1. Both ends (at $x = a$ and $x = b$) are rigidly constrained using kinematic coupling, effectively simulating bonded boundary conditions. A FE study is undertaken with the parameters of Table 2 to produce computational stiffness spectra up to 5 kHz. Typical dynamic stiffness magnitudes in axial, torsional, shear, and flexure are given in Figs. 2–6, respectively. Due to the circular cross-section, the shear-bending properties in the $y - \theta_z$ direction are equivalent in the $z - \theta_y$ direction. Further, the FE and SEM shear/flexure coupling dynamic stiffness spectra for the $L/D = 1$ case are depicted in terms of both magnitude and phase in Fig. 7. Since the aspect ratio changes so significantly, some consideration of the relationship between aspect ratio and frequency range is needed to present appropriate comparison. For example, in the uncoupled directions, the natural frequency (ω_λ) of the continuous system follows $\omega_\lambda \propto 1/L$. Thus, the frequency range of interest relative to the internal modes shifts with the aspect ratio, and so the bandwidth is limited to $\omega \leq L\omega_{max}/D$. This causes the 1/4 aspect ratio to require a 10 kHz frequency range, while higher aspect ratios include a comparable amount of resonance and anti-resonance behavior.

Qualitatively, it is clear from the dynamic stiffness plots that excellent agreement is achieved up to 5 kHz for both the torsional and shear directions. The SEM and FE predictions in the axial, bending, and shear/bending coupling direction all match well up to around the first resonance, and then begin to lose agreement thereafter. One reason for this is that the bonded boundary condition distorts the mode shapes near each end of the elastomeric material—an effect not captured by the spectral element model. Errors magnified in the short aspect ratio are more likely to be related to end-effects. Additionally, the spectral element model assumes slender rod-like behavior in the axial direction. This assumes that displacement is uniform in the cross-section. At high frequencies, longitudinal modes which violate this assumption begin to
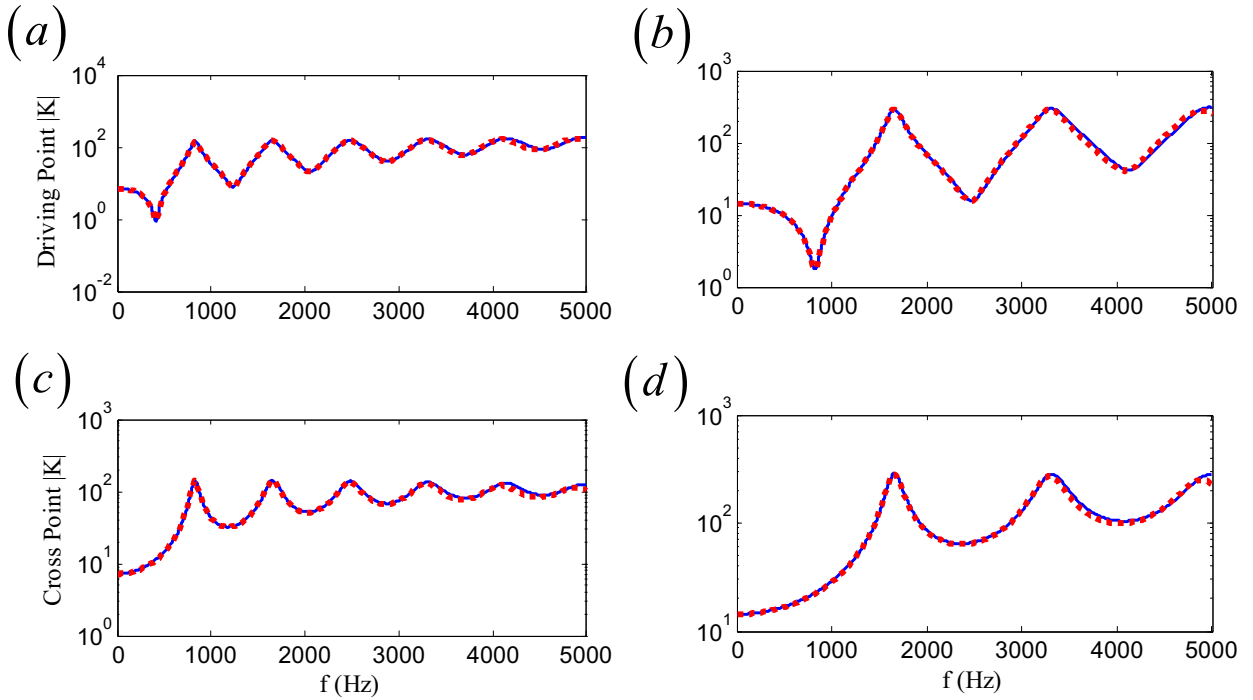
Fig. 3. Torsional dynamic stiffness spectra for the isolator of Fig. 1. With values listed in Table 1. $(a)K_{4a4a}$ with $L/D = 1$, $(b)K_{4a4a}$ with $L/D = 1/2$, $(c)K_{4a4b}$ with $L/D = 1$, $(a)K_{4a4b}$ with $L/D = 1/2$. Key: —— – spectral element model; ∎ ∎ ∎ – finite element model.
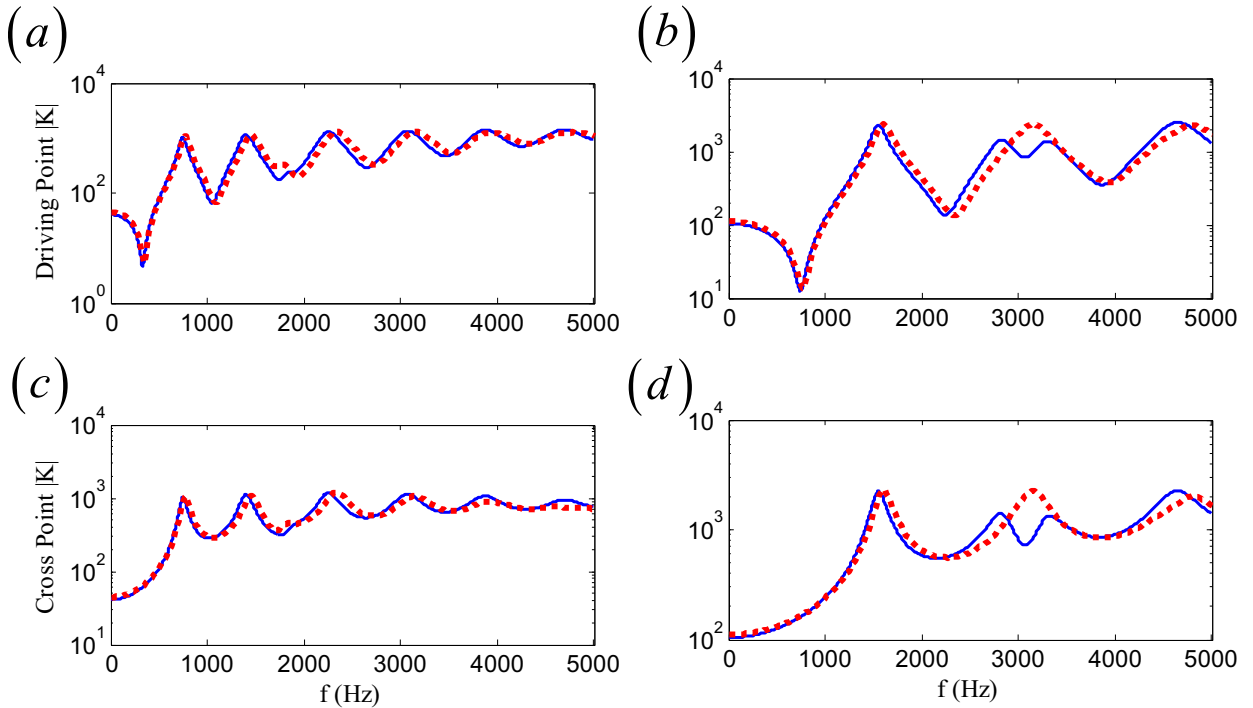

Fig. 4. Shear dynamic stiffness spectra for the isolator of Fig. 1. With values listed in Table 1. $(a)K_{2a2a}$ with $L/D = 1$, $(b)K_{2a2a}$ with $L/D = 1/2$, $(c)K_{2a2b}$ with $L/D = 1$, $(a)K_{2a2b}$ with $L/D = 1/2$. Key: —— – spectral element model; ∎ ∎ ∎ – finite element model.

participate, introducing additional error. Similar effects and errors are present in the bending direction. Finally, many elements are required to preserve accuracy at very high frequencies, and thus some high-frequency errors may be due to insufficient spatial resolution; also, numerical errors are known to exist in the FE method at higher frequencies.

Fig. 5. Shear/flexure coupling dynamic stiffness spectra for the isolator of Fig. 1. With values listed in Table 1. (a)$K_{2a6a} = K_{6a2a}$ with $L/D = 1$, (b)$K_{2a6a} = K_{6a2a}$ with $L/D = 1/2$, (c)$K_{2a6b} = K_{6a2b}$ with $L/D = 1$, (a)$K_{2a6b} = K_{6a2b}$ with $L/D = 1/2$. Key: —— – spectral element model; ▪ ▪ ▪ – finite element model.
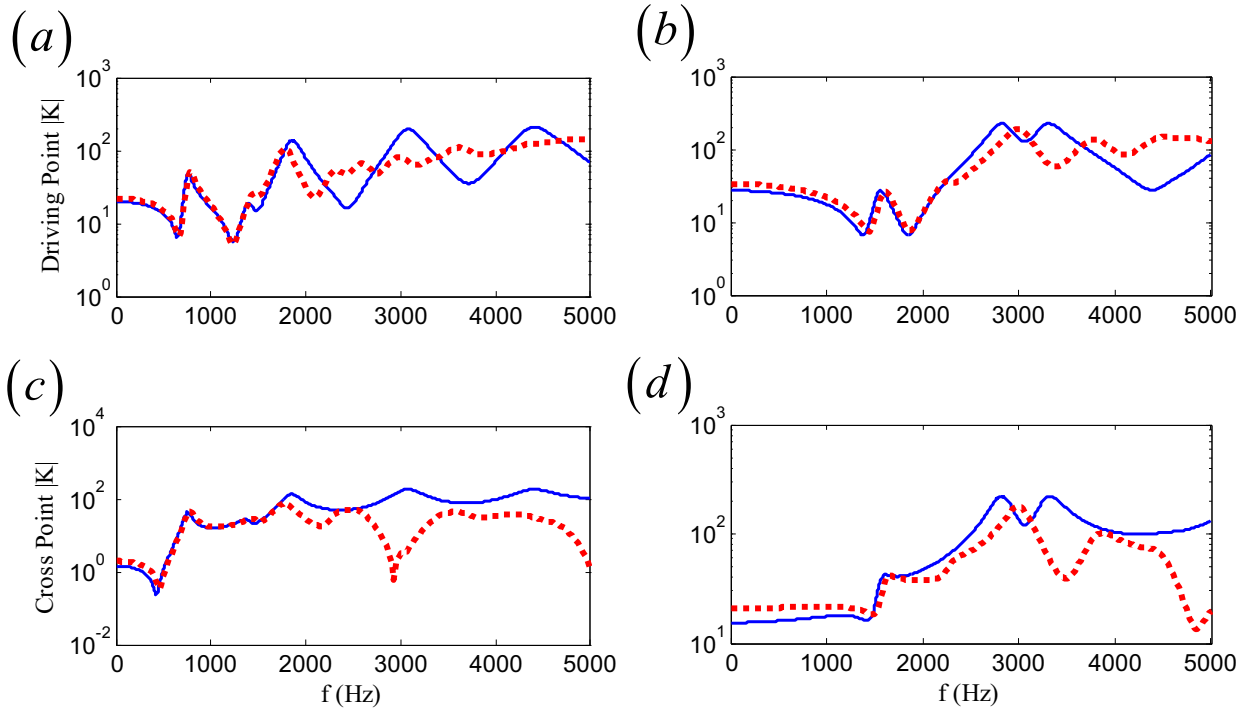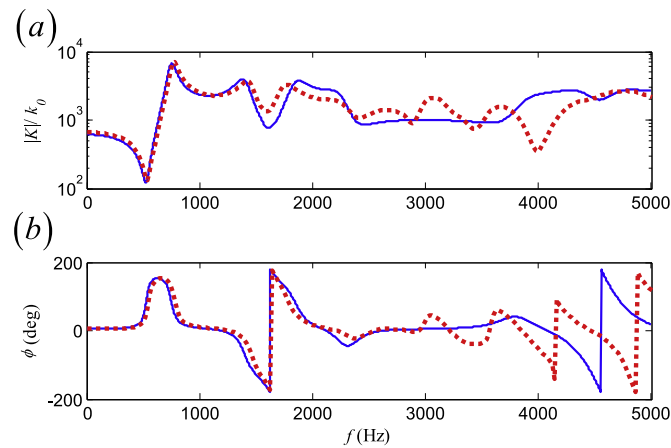

Fig. 6. Flexural dynamic stiffness spectra for the isolator of Fig. 1. With values listed in Table 1. (a)K_{6a6a} with $L/D = 1$, (b)K_{6a6a} with $L/D = 1/2$, (c)K_{6a6b} with $L/D = 1$, (a)K_{6a6b} with $L/D = 1/2$. Key: —— – spectral element model; ▪ ▪ ▪ – finite element model.

Fig. 7. Comparison between SEM and FE predicted dynamic stiffness spectra in terms of (*a*) magnitude and (*b*) phase for the isolator of Fig. 1. With values listed in Table 1. The driving-point shear/flexure coupling term with $L/D = 1$ is used as an illustrative example. Key: ▬▬▬ – spectral element model; ▪ ▪ ▪ – finite element model.

Table 3
Error in the dynamic stiffness magnitudes between finite element (FE) and spectral element method (SEM) predictions as defined by Eq. (46).

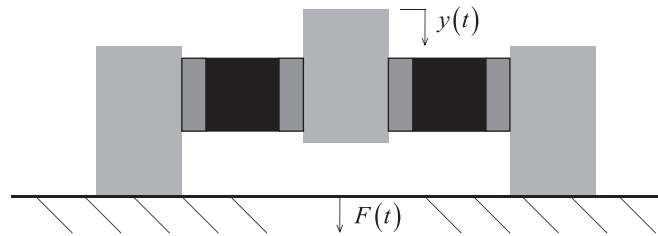| Aspect Ratio (L/D)	Bandwidth (kHz)	Error for Selected Stiffness Term				
		K_{11}	K_{44}	K_{22}	K_{26} or K_{62}	K_{66}
4	0.625	8.1%	8.4%	19.0%	17.8%	16.2%
2	1.25	16.1%	7.0%	22.9%	20.3%	16.6%
1	2.5	50.5%	16.0%	18.6%	24.8%	54.8%
3/4	3.33	51.9%	10.3%	26.6%	35.0%	54.5%
1/2	5	70.8%	15.9%	24.9%	69.0%	56.5%
1/4	10	74.3%	12.3%	27.1%	60.6%	57.2%
Average Error		45.3%	11.7%	23.2%	37.9%	42.6%

Fig. 8. Schematic of the isolator [4] used for experimental validation of spectral element method. Two elastomeric cylindrical elements (as depicted in more detail in Fig. 1) are configured in parallel to ensure that the isolator works in the shear mode. Refer to Table 4 for properties and damping formulation parameters.

Nevertheless, in general, the spectral element model produces reasonable dynamic stiffness predictions compared with finite element predictions.

The discrepancies between FE and SEM magnitudes are quantified using the following percent-difference style error index where the SEM is a benchmark,

$$\varepsilon = \frac{(100\%)}{N} \sum \frac{\left| |\tilde{K}_{FE}| - |\tilde{K}_{SEM}| \right|}{|\tilde{K}_{SEM}|}.$$

(47)

The results of this study are given in Table 3, and several insights emerge. First, certain directions have similar errors at all aspect ratios, including the torsional and shear directions, which vary only minimally. The average error across all aspect ratios is also at a minimum in these two directions, confirming that the SEM assumptions are most reasonable in these directions and thus the predictions are strongest. In the axial, bending, and shear/bending coupling directions, significant dependence on the aspect ratio is observed. The SEM assumptions in these directions become less reasonable as the aspect

Table 4
Properties and parameters used for spectral element model of the isolator of Fig. 8.

Parameter	Damping formulation		
	Fractional	Structural	Viscous
L	25.4 mm	25.4 mm	25.4 mm
D	25.4 mm	25.4 mm	25.4 mm
ρ	1 kg/m^3	1 kg/m^3	1 kg/m^3
ν	0.5	0.5	0.5
E_0	6.2 MPa	12 MPa	12 MPa
η	0.2 s$^{0.17}$	0.13i	1.9×10^{-5} s
α	0.17	0	1

Fig. 9. Experimental validation of the spectral element method for the isolator of Fig. 8. Dynamic stiffness spectra up to 600 Hz are shown in terms of (a) magnitude and (b) phase. Key: ✚ – measurement [4]; ▬▬▬ – finite element model [4]; ▬▬▬ – spectral element model with parameters of Table 4.
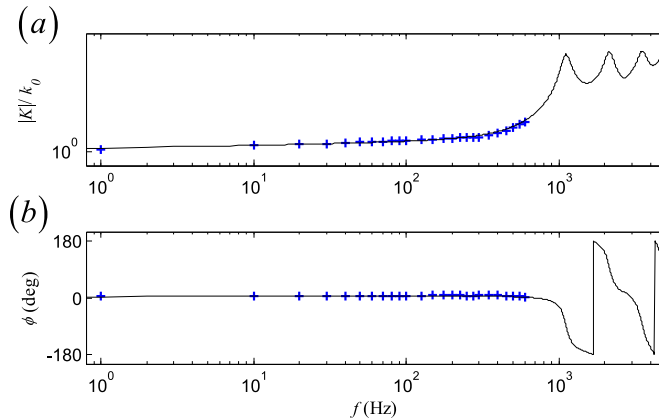

Fig. 10. Experimental validation of the broadband dynamic stiffness for the isolator of Fig. 8 in terms of (a) magnitude and (b) phase. The spectral element model extends the frequency range by an order of magnitude, revealing dynamic behavior not captured in previous computational and experimental studies [4]. Key: ✚ – measurement [4]; ▬▬▬ – finite element model [4]; ▬▬▬ – spectral element model with parameters of Table 4.

ratio is decreased, primarily because the FE model has bonded boundary conditions whereas the SEM assumes free deformation in the cross-sectional plane.

5. Experimental validation

The spectral element approach proposed in this article is particularly useful for a class of isolators which is shown in
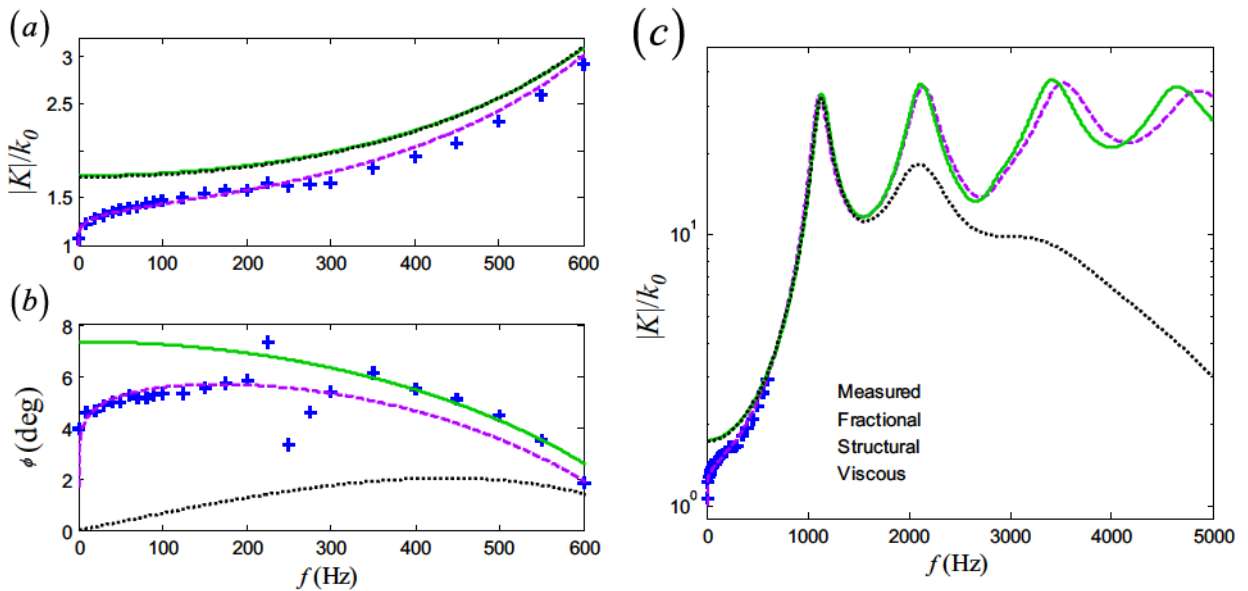
Fig. 11. Experimental validation of the fractional damping formulation when utilized in the spectral element model for the isolator of Fig. 8 in terms of (a) low-frequency dynamic stiffness magnitude, (b) low-frequency loss angle, and (c) broadband dynamic stiffness magnitude. Note comparisons with model predictions when structural or viscous formulation is employed; refer to Table 4 for the parameters used. Key: ✚ – measurement [4]; — · — – fractional damping; ——— – structural damping; ······ – viscous damping.

Fig. 8. Using geometric and other material parameters (as reported in Table 4), the elastic and damping properties are judiciously chosen to simulate the measured dynamic properties of the device as provided in an earlier paper [4]. Since the excitation is purely in the shear direction, the experiment corresponds to the shear direction in the SEM. Thus, $\hat{K}_{SEM} = 2\hat{K}_{2a,2b}$, which is comparable to the measured response.

Over the measured frequency range (up to 600 Hz), the SEM predicted cross-point dynamic stiffness achieves excellent agreement with measurements in terms of both magnitude and phase as demonstrated in Fig. 9. In particular, observe the low frequency trend (as the frequency decreases towards zero), where the magnitudes of measured and spectral element predicted dynamic stiffness converge to the static stiffness, while the structurally damped FE over-predicts the stiffness at lower frequencies. For higher frequencies, measurement of dynamic stiffness becomes increasingly difficult [8], and FE models become computationally expensive. The spectral element model predicts dynamics beyond the measured range as shown in Fig. 10 in a log-scale, illustrating both low- and high-frequency prediction capabilities of the SEM. Additional experimental studies would be necessary to confirm the accuracy at higher frequencies, but this example case provides sufficient validation for the proposed SEM-based approach.

To highlight the benefits of the fractional calculus based damping included in the SEM, the effects of three damping formulations are compared in Fig. 11. A viscous damping mechanism tuned to the first resonance dramatically decays the higher modes and fails to match the measured stiffness magnitude or loss angle at lower frequencies. Structural damping offers reasonable predictions of many modes, but likewise fails to capture the low-frequency behavior.

6. Conclusions

This principal contribution of this article is the development of an analytical spectral element approach to characterize the dynamic properties of viscoelastic vibration isolators up to very high frequencies. It improves the prior literature by extending the stiffness spectra with a fractional calculus based damping mechanism, capturing all 6-DOF including coupling terms, and allowing the isolator to resemble a short beam with $L/D < 1$. The theory is developed from the wave equation assuming longitudinal and torsional waves in a rod alongside the Timoshenko beam theory for shear and flexure, although the method is adaptable to more complicated geometries.

A second contribution of this article is the computational verification and experimental validation of the proposed SEM. Good comparative agreement is achieved while verifying the SEM with FE simulations over a very large frequency range (up to 5 kHz). Since the two methods agree on an order of magnitude basis, the proposed SEM is an improvement in analytical modeling capabilities for cylindrical isolators with short aspect ratios [12]. Compared with experimental characterization of a laboratory isolator, the SEM predicted dynamic stiffness spectra achieve excellent qualitative and quantitative accuracy in terms of both magnitude and phase. In particular, the fractional damping overcomes the inherent limitations of both the viscous and structural damping formulations while capturing the physical phenomena observed in the measured dynamic

stiffness in terms of both magnitude and phase.

Finally, this article adds to the body of knowledge by offering physical insight and providing a compact and elegant method to characterize viscoelastic isolators. And while many elastomeric materials exhibit sensitivity to excitation amplitude, preload, temperature, and material orientation, all of these may be approximated by the linear theory as the starting point since the small amplitude assumption is reasonable over a large frequency bandwidth.

Acknowledgements

References

[1] A.S. Wineman, K.R. Rajagopal, *Mechanical Response of Polymers: An Introduction*, Cambridge University Press, Cambridge, 2000.

[2] L. Kari, The non-linear temperature dependent stiffness of precompressed rubber cylinders-An effective shape factor model, *Kautsch. Gummi Kunststoffe* 55 (2002) 76–81.

[3] M. Sjöberg, L. Kari, Nonlinear isolator dynamics at finite deformations: an effective hyperelastic, fractional derivative, generalized friction model, *Nonlinear Dyn.* 33 (2003) 323–336, http://dx.doi.org/10.1023/A:1026037703124.

[4] S. Noll, B. Joodi, J.T. Dreyer, R. Singh, Volumetric and dynamic performance considerations of elastomeric components, *SAE Int. J. Mater. Manuf.* 8 (2015) 953–959, http://dx.doi.org/10.4271/2015-01-2227.

[5] L. Kari, Dynamic transfer stiffness measurements of vibration isolators in the audible frequency range, *Noise Control Eng. J.* 49 (2001) 88–102, http://dx.doi.org/10.3397/1.2839644.

[6] S. Noll, J.T. Dreyer, R. Singh, Identification of dynamic stiffness matrices of elastomeric joints using direct and inverse methods, *Mech. Syst. Signal Process.* 39 (2013) 227–244, http://dx.doi.org/10.1016/j.ymssp.2013.02.003.

[7] S. Kim, R. Singh, Multi-dimensional characterization of vibration isolators over a wide range of frequencies, *J. Sound Vib.* 245 (2001) 877–913, http://dx.doi.org/10.1006/jsvi.2001.3617.

[8] J.W.R. Meggitt, A.S. Elliott, A.T. Moorhouse, H.K. Lai, In situ determination of dynamic stiffness for resilient elements, *Proc. IMechE Part C: J. Mech. Eng. Sci.* 230 (2016) 986–993, http://dx.doi.org/10.1177/0954406215618986.

[9] N. Gil-Negrete, J. Vinolas, L. Kari, A simplified methodology to predict the dynamic stiffness of carbon-black filled rubber isolators using a finite element code, *J. Sound Vib.* 296 (2006) 757–776, http://dx.doi.org/10.1016/j.jsv.2006.03.038.

[10] E.E. Ungar, C.W. Dietrich, High-frequency vibration isolation, *J. Sound Vib.* 4 (1966) 224–241, http://dx.doi.org/10.1016/0022-460X(66)90123-4.

[11] S. Kim, R. Singh, Vibration transmission through an isolator modeled by continuous system theory, *J. Sound Vib.* 248 (2001) 925–953, http://dx.doi.org/10.1006/jsvi.2001.3852.

[12] M. Östberg, L. Kari, Transverse, tilting, and cross-coupling stiffness of cylindrical rubber isolators in the audible frequency range—the wave-guide solution, *J. Sound Vib.* 330 (2011) 3222–3244, http://dx.doi.org/10.1016/j.jsv.2011.01.020.

[13] J.F. Doyle, *Wave Propagation in Structures*, Springer, New York, 1997.

[14] S. Meng, X.K. Li, G. Evans, Spectral element method for viscoelastic flows in a planar contraction channel, *Int. J. Numer. Methods Fluids* 42 (2003) 323–348, http://dx.doi.org/10.1002/d.524.

[15] D. Komatitsch, J. Tromp, Introduction to the spectral element method for three-dimensional seismic wave propagation, . *Geophys. J. Int.* 139 (1999) 806–822, http://dx.doi.org/10.1046/j.1365-246x.1999.00967.x.

[16] U. Lee, Equivalent continuum representation of lattice beams: spectral element approach, *Eng. Struct.* 20 (1998) 587–592, http://dx.doi.org/10.1016/S0141-0296(97)00063-1.

[17] U. Lee, Vibration analysis of one-dimensional structures using the spectral transfer matrix method, *Eng. Struct.* 22 (2000) 681–690, http://dx.doi.org/10.1016/S0141-0296(99)00002-4.

[18] A.M. Horr, M. Safi, N. Asadpour, Seismic analysis of Tehran telecommunication tower using complex fractional modulus, *Struct. Des. Tall Spec. Build.* 11 (2002) 353–373, http://dx.doi.org/10.1002/tal.206.

[19] A.M. Horr, M. Safi, Impact wave propagation in tall buildings using advanced spectral element method, *Struct. Des. Tall Spec. Build.* 12 (2003) 127–143, http://dx.doi.org/10.1002/tal.217.

[20] R. Herrmann, *Fractional Calculus: An Introduction for Physicists*, World Scientific, 2014.

[21] R.L. Bagley, R.A. Calico, Fractional order state equations for the control of viscoelastically damped structures, *J. Guid., Control, Dyn.* 14 (1991) 304–311, http://dx.doi.org/10.2514/3.20641.

[22] J.C. Snowdon, Mechanical four-pole parameters and their application, *J. Sound Vib.* 15 (1971) 307–323, http://dx.doi.org/10.1016/0022-460X(71)90427-5.

[23] G.R. Cowper, The shear coefficient in Timoshenko's beam theory, *J. Appl. Mech.* 33 (1966) 335–340, http://dx.doi.org/10.1115/1.3625046.